CHEMISTRY OF MATERIALS
Article

Chem. Mater. **2010,** *22,* 5003–5012 5003
DOI:10.1021/cm1012729

Ionic Liquid Monomers and Polymers as Precursors of Highly Conductive, Mesoporous, Graphitic Carbon Nanostructures

Jiayin Yuan,* Cristina Giordano, and Markus Antonietti

Max-Planck-Institute of Colloids and Interfaces, Department of Colloid Chemistry, Research Campus Golm, Am Muehlenberg 1, D-14476 Golm, Germany

Received May 6, 2010. Revised Manuscript Received July 20, 2010

In this contribution a template-free preparation of mesoporous graphitic carbon nanostructures with high electric conductivity is presented, using ionic liquid monomers or poly(ionic liquid) polymers as carbon precursors. The carbonization was performed in the presence of $FeCl_2$ at temperatures between 900 and 1000 °C. It was found that $FeCl_2$ plays a key role in controlling both the chemical structure and the texture morphology of the graphitization process. A detailed investigation on the carbonization process demonstrated that 900 °C is a threshold temperature where a synergistic formation process enables the development of the superior physical properties, such as large surface area and low resistance. The as-synthesized carbon products are graphitic, mesoporous, and highly conductive, as proven by XRD and TEM characterizations and conductivity measurements. Via an acid etching process, iron and iron carbide nanoparticles, the remainder of the primary catalyst, can be removed, leaving pure mesoporous carbon nanomaterials with a comparably well developed graphitic structure. Without demand for any template, this method is facile and easy to scale up and might contribute to the wide range of applications of carbon nanostructures.

1. Introduction

There is rapidly expanding interest in mesoporous carbon materials with large surface area due to their promising applications as adsorbents for adsorption and separation processes,[1−4] as a supporting matrix for catalysts in fuel cells,[5−7] as hydrogen storage materials,[8] as electrochemical double-layer capacitors,[9] and as electrode materials in lithium batteries,[10,11] just to name a few. To date, several methods have been developed to synthesize mesoporous carbons.[12,13] Among these, we can cite (1) the catalytic activation of carbon precursors in the presence of metals and organometallic components,[14] (2) high temperature activation by physical or combined physical/chemical methods,[15] (3) carbonization of polymer blends with one thermally unstable component,[16] (4) carbonization of polymer aerogels such as resorcinol−formaldehyde resins under rearrangements of the carbon scaffold,[17] (5) self-assembly using soft templates through cocondensation and carbonization,[18−22] and (6) replication synthesis with presynthesized hard templates through an impregnation−carbonization−template removal procedure.[23−30]

In spite of the significant accomplishments that have been reached, the pursuit of complementary synthetic

*Corresponding author. E-mail: jiayin.yuan@mpikg.mpg.de.

(1) Vinu, A.; Miyahara, M.; Sivamurugan, V.; Mori, T.; Ariga, K. *J. Mater. Chem.* **2005**, *15*(48), 5122–5127.
(2) Vinu, A.; Hossain, K. Z.; Kumar, G. S.; Ariga, K. *Carbon* **2006**, *44* (3), 530–536.
(3) Han, S.; Sohn, K.; Hyeon, T. *Chem. Mater.* **2000**, *12*(11), 3337–3341.
(4) Vinu, A.; Hossian, K. Z.; Srinivasu, P.; Miyahara, M.; Anandan, S.; Gokulakrishnan, N.; Mori, T.; Ariga, K.; Balasubramanian, V. V. *J. Mater. Chem.* **2007**, *17*(18), 1819–1825.
(5) Joo, S. H.; Choi, S. J.; Oh, I.; Kwak, J.; Liu, Z.; Terasaki, O.; Ryoo, R. *Nature* **2001**, *412*(6843), 169–172.
(6) Chang, H.; Joo, S. H.; Pak, C. *J. Mater. Chem.* **2007**, *17*(30), 3078–3088.
(7) Nam, J.-H.; Jang, Y.-Y.; Kwon, Y.-U.; Nam, J.-D. *Electrochem. Commun.* **2004**, *6*(7), 737–741.
(8) Yang, Z.; Xia, Y.; Mokaya, R. *J. Am. Chem. Soc.* **2007**, *129*(6), 1673–1679.
(9) Yoon, S.; Lee, J.; Hyeon, T.; Oh, S. M. *J. Electrochem. Soc.* **2000**, *147*(7), 2507–2512.
(10) Zhou, H.; Zhu, S.; Hibino, M.; Honma, I.; Ichihara, M. *Adv. Mater.* **2003**, *15*(24), 2107–2111.
(11) Fan, J.; Wang, T.; Yu, C.; Tu, B.; Jiang, Z.; Zhao, D. *Adv. Mater.* **2004**, *16*(16), 1432–1436.
(12) Liang, C.; Li, Z.; Dai, S. *Angew. Chem., Int. Ed.* **2008**, *47*(20), 3696–3717.
(13) Stein, A. *Adv. Mater.* **2003**, *15*(10), 763–775.
(14) Kyotani, T. *Carbon* **2000**, *38*(2), 269–286.
(15) Hu, Z.; Srinivasan, M. P.; Ni, Y. *Adv. Mater.* **2000**, *12*(1), 62–65.
(16) Patel, N.; Okabe, K.; Oya, A. *Carbon* **2002**, *40*(3), 315–320.
(17) Pekala, R. W. *J. Mater. Sci.* **1989**, *24*(9), 3221–7.
(18) Meng, Y.; Gu, D.; Zhang, F.; Shi, Y.; Cheng, L.; Feng, D.; Wu, Z.; Chen, Z.; Wan, Y.; Stein, A.; Zhao, D. *Chem. Mater.* **2006**, *18*(18), 4447–4464.
(19) Meng, Y.; Gu, D.; Zhang, F.; Shi, Y.; Yang, H.; Li, Z.; Yu, C.; Tu, B.; Zhao, D. *Angew. Chem., Int. Ed.* **2005**, *44*(43), 7053–7059.
(20) Zhang, F.; Meng, Y.; Gu, D.; Yan, Yu, C.; Tu, B.; Zhao, D. *J. Am. Chem. Soc.* **2005**, *127*(39), 13508–13509.
(21) Zhang, F.; Meng, Y.; Gu, D.; Yan; Chen, Z.; Tu, B.; Zhao, D. *Chem. Mater.* **2006**, *18*(22), 5279–5288.
(22) Deng, Y.; Yu, T.; Wan, Y.; Shi, Y.; Meng, Y.; Gu, D.; Zhang, L.; Huang, Y.; Liu, C.; Wu, X.; Zhao, D. *J. Am. Chem. Soc.* **2007**, *129* (6), 1690–1697.
(23) Fan, W.; Snyder, M. A.; Kumar, S.; Lee, P.-S.; Yoo, W. C.; McCormick, A. V.; Lee Penn, R.; Stein, A.; Tsapatsis, M. *Nature Mater.* **2008**, *7*(12), 984–991.
(24) Wang, Z.; Kiesel, E. R.; Stein, A. *J. Mater. Chem.* **2008**, *18*(19), 2194–2200.
(25) Wang, Z.; Li, F.; Stein, A. *Nano Lett.* **2007**, *7*(10), 3223–3226.
(26) Wang, Z.; Li, F.; Ergang, N. S.; Stein, A. *Chem. Mater.* **2006**, *18* (23), 5543–5553.
(27) Anandan, S.; Vinu, A.; Mori, T.; Ariga, K. *Trans. Mater. Res. Soc. Jpn.* **2007**, *32*(4), 1003–1005.

Published on Web 08/09/2010

strategies toward mesoporous carbon materials with extreme performance values remains the focus of current research, as many applications of mesoporous carbon materials are related not only to the high surface area but also to their superior physical and chemical properties, such as electric conductivity, thermal conductivity, chemical stability, and, last but not least, practically unlimited availability.

In contrast to amorphous or disordered carbon, graphitized carbons with the well-developed local crystalline structure exhibit high electric conductivity and improved chemical or electrochemical stability. For example, the Pt and SnO_2 catalyst loaded on graphitized carbon showed improved activity for methanol oxidation, good rate capability, and good cyclability in Li-ion storage.[31−35] Thus, from the viewpoint of the electrochemical application, graphitized mesoporous carbons with high crystallinity and relatively large surface area are more desired. Mesoporous graphitized carbons have been prepared commonly through a template-directed approach, for example, mesoporous SBA-15[36] or silica colloids,[30] from carbon sources including polyaromatic hydrocarbons,[36,37] polyacrylonitrile,[38,39] mesophase pitches,[40] acetonitrile,[41] benzene,[42] etc. Recently, the catalytic graphitization has been proven to be an effective means to prepare graphitic carbon with higher crystallinity under mild conditions. With the aid of catalyst, porous carbon containing graphitic structure could be obtained at relatively low pyrolysis temperature using metal salt impregnated mesoporous silica as template.[43−45] The main drawback associated with template-directed synthesis is the template production, which is often time-consuming and, in some cases, costly. This limits its cost-effective production on a large scale. A template-free synthetic approach is thus mightily demanded; however, the preparation of mesoporous graphitic carbon has been rarely reported.[46]

Very recently, ionic liquids (ILs) have been applied for the synthesis of mesoporous N-doped graphitic carbon at 1000 °C in a SBA-15 template.[47] The discriminating advantage of the ionic liquid is to start from a nonvolatile precursor which is keeping a high mass yield until the onset of decomposition processes which in addition can be printed, coated, or structured and molded (polymer). In this contribution we report a template-free synthesis of highly conductive, mesoporous, graphitic carbon nanostructures using ionic liquid monomers or poly(ionic liquid) polymers as carbon precursors in the presence of $FeCl_2 \cdot 4H_2O$. It was found that the iron salt played a key role in conducting the graphitization process at a moderate temperature (900−1000 °C). A detailed investigation on the carbonization process demonstrates that 900 °C is the threshold temperature at which the superior physical properties develop, such as high surface area and low resistance. The as-synthesized carbon products consist of small, crumpled/folded stacks of sheetlike graphitic nanostructures. The overall structure is mesoporous and more conductive than that of commercial graphite, which is due to heterojunction-doping with iron and iron carbide nanoparticles dispersed in the graphitic matrix, as proven by XRD and TEM characterization. Via an acid etching process assisted by ultrasound, iron and iron carbide nanoparticles could be removed, leaving pure mesoporous graphitic nanomaterials. As an advantage of its facile implementation, this synthesis is easy to scale up and shows the potential for wider variability.

2. Experimental Section

Materials. $FeCl_2 \cdot 4H_2O$ (Aldrich 98%), 1-vinylimidazole (Aldrich 99%), bromoethane (Aldrich 98%), bromoacetonitrile (Aldrich 97%), 4-bromobutyronitrile (Aldrich 97%), $CrCl_3 \cdot 6H_2O$(Aldrich 99%), and graphite powders (Aldrich) were used as received without further purifications. 2,2′-Azobis(2-methylpropionitrile) (Aldrich 98%) was recrystallized from methanol. Silver dicyanamide and IL monomers (IL-a, 1-vinyl-3-ethylimidazolium bromide; IL-b, 1-vinyl-3-ethylimidazolium dicyanamide; IL-c, 1-vinyl-3-cyanomethylimidazolium bromide; and IL-d, 1-vinyl-3-cyanopropylimidazolium bromide; see Figure 1 for chemical structures) were prepared similarly according to previous literature.[47−49]

Preparation of Poly(ionic liquid) Polymers. PIL-a: 10.38 g of IL-a (50.8 mmol), 30 mg of AIBN (0.183 mmol), and 70 mL of ethanol were loaded into a 250 mL of reactor. The mixture was deoxygenated three times by a freeze−pump−thaw procedure. The reactor was then refilled with nitrogen and placed in an oil bath at 70 °C for 24 h. The mixture was then exhaustively dialyzed against water for 1 week and freeze-dried from water.

(28) Yu, C.; Fan, J.; Tian, B.; Zhao, D.; Stucky, G. D. *Adv. Mater.* **2002**, *14*(23), 1742–1745.
(29) Logudurai, R.; Anand, C.; Balasubramanian, V. V.; Ariga, K.; Srinivasu, P.; Vinu, A. J. Nanosci. Nanotechnol. *10*, (1), 329−335.
(30) Lei, Z.; Xiao, Y.; Dang, L.; Bai, S.; An, L. *Microporous Mesoporous Mater.* **2008**, *109*(1−3), 109–117.
(31) Zeng, J.; Su, F.; Han, Y.-F.; Tian, Z.; Poh, C. K.; Liu, Z.; Lin, J.; Lee, J. Y.; Zhao, X. S. *J. Phys. Chem. C* **2008**, *112*(40), 15908–15914.
(32) Zeng, J.; Su, F.; Lee, J. Y.; Zhao, X. S.; Chen, J.; Jiang, X. *J. Mater. Sci.* **2007**, *42*(17), 7191–7197.
(33) Wang, Y.; Su, F.; Lee, J. Y.; Zhao, X. S. *Chem. Mater.* **2006**, *18*(5), 1347–1353.
(34) Su, F.; Zhao, X. S.; Wang, Y.; Zeng, J.; Zhou, Z.; Lee, J. Y. *J. Phys. Chem. B* **2005**, *109*(43), 20200–20206.
(35) Su, F.; Zeng, J.; Bao, X.; Yu, Y.; Lee, J. Y.; Zhao, X. S. *Chem. Mater.* **2005**, *17*(15), 3960–3967.
(36) Kim, T.-W.; Park, I.-S.; Ryoo, R. *Angew. Chem., Int. Ed.* **2003**, *42* (36), 4375–4379.
(37) Kim, C. H.; Lee, D.-K.; Pinnavaia, T. J. *Langmuir* **2004**, *20*(13), 5157–5159.
(38) Kruk, M.; Dufour, B.; Celer, E. B.; Kowalewski, T.; Jaroniec, M.; Matyjaszewski, K. *J. Phys. Chem. B* **2005**, *109*(19), 9216–9225.
(39) Lu, A.; Kiefer, A.; Schmidt, W.; Schueth, F. *Chem. Mater.* **2004**, *16* (1), 100–103.
(40) Li, Z.; Jaroniec, M. *J. Phys. Chem. B* **2004**, *108*(3), 824–826.
(41) Xia, Y.; Mokaya, R. *Adv. Mater.* **2004**, *16*(17), 1553–1558.
(42) Su, F.; Zhao, X. S.; Wang, Y.; Lee, J. Y. *Microporous Mesoporous Mater.* **2007**, *98*(1−3), 323–329.
(43) Fuertes, A. B.; Centeno, T. A. *J. Mater. Chem.* **2005**, *15*(10), 1079–1083.
(44) Yang, C.-M.; Weidenthaler, C.; Spliethoff, B.; Mayanna, M.; Schueth, F. *Chem. Mater.* **2005**, *17*(2), 355–358.
(45) Ji, X.; Herle, P. S.; Rho, Y.; Nazar, L. F. *Chem. Mater.* **2007**, *19*(3), 374–383.
(46) Yasuda, H.; Miyanaga, S.; Nakamura, A.; Sakai, H. *J. Inorg. Organomet. Polym.* **1991**, *1*(1), 135–41.
(47) Paraknowitsch, J. P.; Zhang, J.; Su, D.; Thomas, A.; Antonietti, M. *Adv. Mater.* **2010**, *22*(1), 87–92.
(48) Gao, Y.; Gao, H.; Piekarski, C.; Shreeve, J. n. M. *Eur. J. Inorg. Chem.* **2007**, *31*, 4965–4972.
(49) Salamone, J. C.; Israel, S. C.; Taylor, P.; Snider, B. *Polymer* **1973**, *14*(12), 639–44.

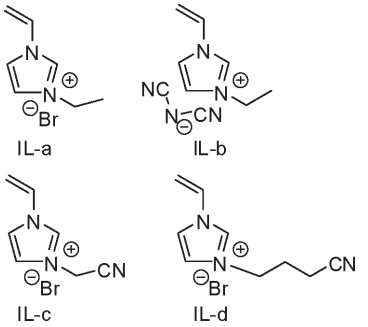

Figure 1. Chemical structures of four imidazolium-based IL monomers used as carbon precursors.

PIL-b was prepared and purified in a similar procedure, except using DMF instead of ethanol as the polymerization solvent.

Carbonization Process. In a typical experiment, 400 mg of IL monomer in 1 mL of ethanol or PIL polymer in 2 mL of water was loaded into an alumina crucible. The mixture was stirred until a homogeneous mixture was obtained. Gentle heating was necessary for the dissolution of PIL-b polymer. For carbonization of IL with iron precursor, 12 wt % (with regard to the IL) of $FeCl_2 \cdot 4H_2O$ was added. The mixture was stirred further for 5 min to obtain a homogeneous mixture. In the case of $FeCl_2 \cdot 4H_2O$ with IL-a, IL-c, or PIL-a, 1−2 mL of water was added additionally to dissolve the precipitate. It must be said that an inhomogeneous mixing of $FeCl_2 \cdot 4H_2O$ with IL monomers or polymers leads to a decrease in the surface area of the carbon product, so homogenization is mandatory. The crucible was then placed in an oven. The sample was heated up to 1000 °C (100 °C/h) and maintained at the final temperature for 2 h under a nitrogen atmosphere. Afterward, the oven was slowly cooled down to room temperature (ca. 14 h).

HCl-Etching Process. In order to remove the iron and iron compounds, the solid carbon products were finely ground for 10 min, dispersed into 4 mL of an aqueous solution of HCl (37 wt %), and kept under stirring overnight. The carbon powder was then separated by ultracentrifugation from the yellow supernatant, washed several times with deionized water, and dried under high vacuum at 120 °C overnight.

The dried powder was ground again for 10 min and redispersed in 20 mL of dioxane. The mixture was treated with ultrasound for 10 min at 60% amplitude (Branson sonifier W450 Digital, mode: 2 s on and 4 s off). Two milliliters of aqueous solution of HCl (37 wt %) was added to the dispersion immediately after the ultrasound treatment, and the mixture was placed in a normal ultrasonic bath for a further 1 h. The carbon powder was separated by ultracentrifugation and washed several times with dioxane and dried under high vacuum at 120 °C overnight.

This purification process was repeated one more time in ethanol.

Characterization Methods. X-ray diffraction patterns were recorded on a Bruker D8 diffractometer using Cu Kα radiation ($\lambda = 0.154$ nm) and a scintillation counter.

Nitrogen sorption experiments were performed with a Quantachrome Autosorb-1 or Quadrasorb at liquid nitrogen temperature, and data analysis was performed with Quantachrome software. The surface area was calculated using the BET equation. The pore size distribution was calculated using the Barrett−Joyner−Halenda (BJH) method. The samples were degassed at 120 °C for 15 h before measurements.

Elemental analysis was performed for carbon, hydrogen, and nitrogen using a Vario EL Elementar.

Transmission electron microscopy (TEM) images were taken on a Zeiss EM 912 Ω operated at an acceleration voltage of 120 kV. Samples were ground, suspended in ethanol, and treated with medium sonication (up to 2 min at 55% amplitude in 30 s doses, with a microtip using a Branson W-450D sonifier) to get a homogeneous suspension. One drop of this suspension was put on a 400 mesh carbon-coated copper grid and left in air to dry.

High-resolution TEM images were taken on a Philips CM 200 LaB_6, operated at an acceleration voltage of 200 kV.

Conductivity measurements were performed by confining the sample between two platinum discs and measuring the electrical resistance of the sample by electric impedance spectroscopy. A Gamry Reference 600 potentiostat system was used.

3. Results and Discussion

Pyrolysis of imidazolium-based IL monomers and poly(ionic liquid) (PIL) polymers in the presence of iron salt, $FeCl_2 \cdot 4H_2O$, allowed preparation of mesoporous graphitic carbon materials in general. Four types of IL compounds, 1-vinyl-3-ethylimidazolium bromide (IL-a), 1-vinyl-3-ethylimidazolium dicyanamide (IL-b), 1-vinyl-3-cyanomethylimidazolium bromide (IL-c), and 1-vinyl-3-cyanopropylimidazolium bromide (IL-d), were chosen in our study. Their chemical structures are provided in Figure 1. An unusual feature of these IL compounds is each bears a polymerizable vinyl group. Therefore, they are also monomers that can be polymerized into PIL polymers, which also enables us to compare the influence of molecular weight and coupled viscosity on the carbon structure.

As is well-known, the key structural prerequisite of polymeric precursors to enable high carbon yields (atom efficiency toward the desired carbon structure) is—besides a neglibible vapor pressure at elevated temperatures—the presence of certain functional groups that undergo cross-linking reactions under pyrolytic conditions. The cyano or nitrile group is the widely employed function that gives high carbon yield under charring conditions.[50,51] Correspondingly, in our study, IL-b, IL-c, and IL-d IL monomers possess a nitrile functionality either in the cation or anion, except IL-a, the precursor of IL-b, which we use as a reference compound without any nitrile group.

The IL monomers were carbonized by heating the samples in alumina crucibles under nitrogen atmosphere up to 1000 °C (heating rate: 100 °C/h) and keeping at this temperature for 2 h. The characterizations and analysis results of the carbon products are summarized in Table 1. Results on the corresponding polymers will be discussed at the end of the paper.

It is interesting to calculate an effective "carbon yield", i.e. the amount of carbon atoms in condensable groups (not in leaving groups) really ending up in the final carbon structure. This teaches us much more about the mechanism

(50) Lee, J. S.; Wang, X.; Luo, H.; Baker, G. A.; Dai, S. *J. Am. Chem. Soc.* **2009**, *131*(13), 4596–4597.
(51) Lee, J. S.; Wang, X.; Luo, H.; Dai, S. Adv. Mater. *22*, (9), 1004−1007.

Table 1. Characterization of Carbon Products of IL-a, IL-b, IL-c, and IL-d Obtained at 1000 °C

	without $FeCl_2 \cdot 4H_2O$			with $FeCl_2 \cdot 4H_2O$ (12 wt %)		
samples[a]	oven yield (%)	surface area (m^2/g)	relative specific resistance[b]	oven yield (%)	surface area (m^2/g)	relative specific resistance
IL-a	6.5	< 10	1.66	14.3	226	0.46
IL-b	28.6	< 10	0.80	29.7	170	0.67
IL-c	29.0	< 10	2.16	27.9	154	0.68
IL-d	14.3	< 10	1.31	21.7	172	0.53

[a] IL structural details are provided in Figure 1. [b] The relative specific resistance is obtained by comparing the measured specific resistance of the carbon products with that of the graphite reference.

and the efficiency of the process than the mass yield, which is expectedly low. As a first assumption, it can be taken that only the carbon atoms in the sp^2 or sp hybrid state can be incorporated into the graphitic structure, while the others form, via fragmentation, low molecular weight gases (typically alkenes arising from alkyl fragmentation). The interesting cases are the carbon atoms in the vinyl group that can turn into a sp^3 state due to thermal polymerization under carbonization conditions. Therefore, the monomers (from IL-a to IL-d) have 3, 6, 4, and 4 carbons, respectively, which can be assumed to end up to construct the corresponding carbon products. Then, a 100% atom efficiency would result in a theoretical oven yield of 17.7% (IL-a), 31.7% (IL-b), 22.4% (IL-c), and 19.8% (IL-d). Comparing these values with the real oven yield (Table 1), the truly atom efficiency is 37% for IL-a, 90% for IL-b, 129% for IL-c, and 72% for IL-d, respectively. The reference compound IL-a gives the lowest yield and atom efficiency, as it lacks the nitrile group that was found to be a key element in higher thermal condensation. In comparison, IL-b, IL-c, and IL-d show satisfactory oven yields and atom efficiencies. The atom efficiency of IL-c exceeds 100%; this clearly teaches us that additional carbon atoms can be activated to be included in the final graphitic structures. Here, it is supposed that the acidic methylene group (-CH_2-) between the cyano group and the imidazolium cation was activated and incorporated into the carbon framework at the carbonization temperatures. From these data, we can therefore state that both replacing Br with dicyanamide as well as using the cyanomethyl group for alkylation are effective ways to increase the atom efficiency of carbonization and thereby the relative shrinkage of the material throughout carbonization.

The carbon products derived from IL monomers without added iron show only limited surface area (S_{BET} < 10 m^2/g), as shown by the nitrogen adsorption measurements. This is in good agreement with previous work on the uncatalyzed carbonization of other IL monomers[47] and speaks for the existence of sufficient liquidlike mobility at the fragmentation temperature to enable sintering and shrinking. The nonporous nature of the carbon products is in accordance with the observation in TEM characterization. Figure 2A is a representative TEM image of the carbon product obtained from IL-b. No inner pore system could be detected. The specific resistance of the carbon products was measured and compared with that of commercial graphite powder as reference.

In spite of the applied medium range temperatures (note that efficient graphitization usually relies on temperatures of 2000 °C and above), it is interesting that these N-doped carbons nevertheless offer a rather high electric conductivity. One of the carbon products, IL-b (relative specific resistance: 0.80), even exhibits a lower resistance than the graphite reference. This agrees with our recent research finding that imidazolium-based IL compound with a dicyanamide anion through pyrolysis at 1000 °C showed better conductivity than graphite.[47] But also the other substances are at least of the order of graphite and favorably compete with conduction soots.

As reported, iron and iron compounds have been frequently employed as catalyst during the carbonization process to promote the formation of graphitic structures from amorphous carbon at a moderate temperature.[46,52−55] In our attempt, when $FeCl_2 \cdot 4H_2O$ as iron source was added to the IL monomers in a weight fraction of 12%, dramatic changes in morphology and properties were observed in the carbon products. This is most straightforwardly reflected in a large BET surface area of 150 −220 m^2/g (Table 1), as determined by nitrogen sorption measurements, which is mostly due to the development of a technologically applicable mesopore system. To understand the origin of the large surface area, TEM characterization of the carbon products was performed. The results are shown in Figure 2. Unlike the Figure 2A reference without added $FeCl_2$, the TEM images of the carbon products exhibit nanoscopic fine structures in the bulk. Closer views reveal a folded, lamellar-like morphology of stiff graphite plates with thicknesses in the range 5−20 nm. In these images, the specific starting products seem to have some influence on the formed carbon nanostructure: while relatively flat carbon sheets seem to be produced from IL-a (Figure 2B) and IL-d (Figure 2F), more curved and wrapped structures are obtained in the case of IL-b (Figure 2C and D) and IL-c (Figure 2 E). The intrinsic nature of these lamellar layers is studied by high-resolution TEM (HRTEM) characterization. Figure 3A shows the HRTEM image of a curved sheet in the carbon product from IL-b with an iron source at 1000 °C. As clearly revealed, the lamellar-like structures are in fact layered graphitic nanostructures, constructed from the stacking of graphene sheets with a *d* spacing of 0.338 ± 0.002 nm. This value matches well with the one

(52) Maldonado-Hodar, F. J.; Moreno-Castilla, C.; Rivera-Utrilla, J.; Hanzawa, Y.; Yamada, Y. *Langmuir* **2000**, *16*(9), 4367–4373.
(53) Lei, Z.; Xiao, Y.; Dang, L.; You, W.; Hu, G.; Zhang, J. *Chem. Mater.* **2007**, *19*(3), 477–484.
(54) Sevilla, M.; Fuertes, A. B. *Carbon* **2006**, *44*(3), 468–474.
(55) Rodriguez, N. M.; Chambers, A.; Baker, R. T. K. *Langmuir* **1995**, *11*(10), 3862–6.

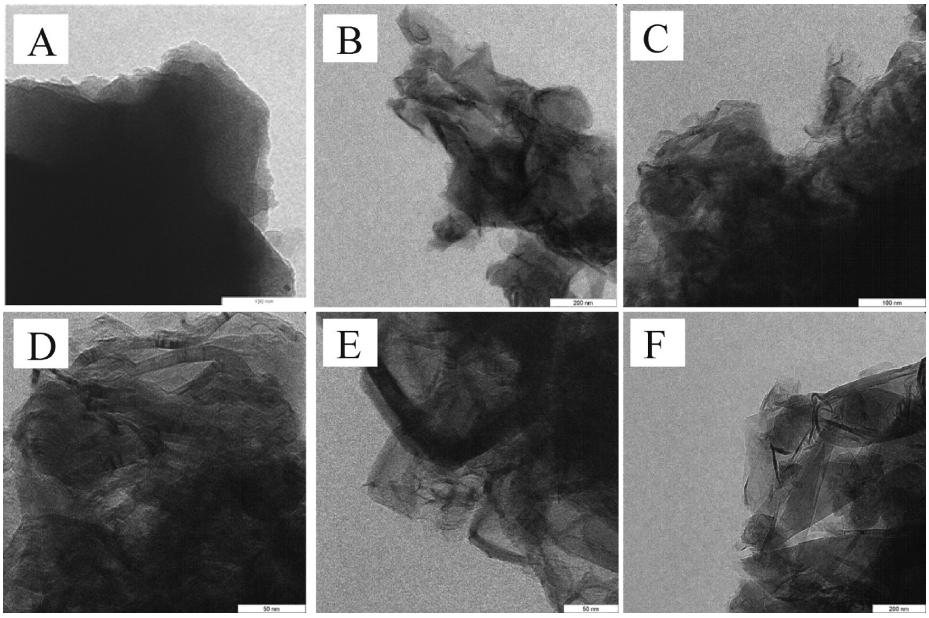

Figure 2. Representative TEM images of carbon products derived from (A) IL-b, (B, C, E, F) IL-a, IL-b, IL-c, and ILd with 12 wt % of $FeCl_2 \cdot 4H_2O$ at 1000 °C, respectively. Part D is an enlarged view of part C. The scale bars in A−F are 100, 200, 100, 50, 50, and 200 nm, respectively.

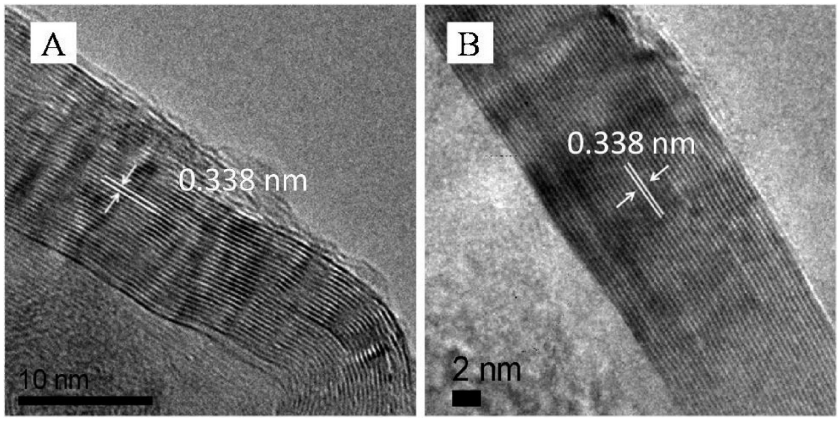

Figure 3. HRTEM images of the carbon product from IL-b with 12 wt % $FeCl_2 \cdot 4H_2O$ pyrolyzed at 1000 °C before (A) and after (B) removal of iron species via an HCl etching process.

expected for graphitic structures reported.[52] Even compared to microparticles of synthetic graphite, the products are highly conductive. As shown in Table 1, all four ILs after carbonization in the presence of $FeCl_2 \cdot 4H_2O$ give significantly lower relative resistance than graphite. Also compared to their corresponding carbon products synthesized in the absence of iron source, the conductivity has remarkably increased.

In our opinion, the enhanced conductivity is brought about from two main factors: (1) the highly developed graphitic nanostructures themselves give a very good charge carrier mobility; (2) as compared to graphite, there must be extra charge carriers in the system. These could be due to heterojunction contacts with metallic iron and iron carbide nanoparticles (10 − 80 nm) in the carbon products, as proven in the TEM characterization (Figure S1 in the Supporting Information) and X-ray diffraction (XRD) analysis down below. It is well-known that such polarizing interfaces can create extra charge carriers,[56] which then contribute to the overall conductivity of the binary hybrid system.

Since all these carbon products are graphitic, the doping and the connected conductivity are mainly dominated by the amount of interface area toward iron and iron carbide species. Starting from the same amount of IL monomers, the amount of iron and iron carbide in the carbon products decreases with the oven yields. Correspondingly, the relative resistance increases in the same sequence, IL-a < IL-d < IL-b ~ IL-c.

To learn about the kinetic details of the formation of this unusual structure, the temperature-dependent structural evolution of graphitic carbon from IL monomers in the presence of $FeCl_2$ was investigated. IL-b was chosen as a model IL monomer for reason of the superior conductivity of its carbon product either with or without iron source. Instead of 1000 °C, we repeated the carbonization of IL-b with $FeCl_2 \cdot 4H_2O$ at temperatures ranging from 800 to 950 °C with an interval of 50 °C.

(56) Hu, Y.-S.; Liu, X.; Müller, J. O.; Schlögl, R.; Maier, J.; Su, D. S. *Angew. Chem., Int. Ed.* **2009**, *48*(1), 210–214.

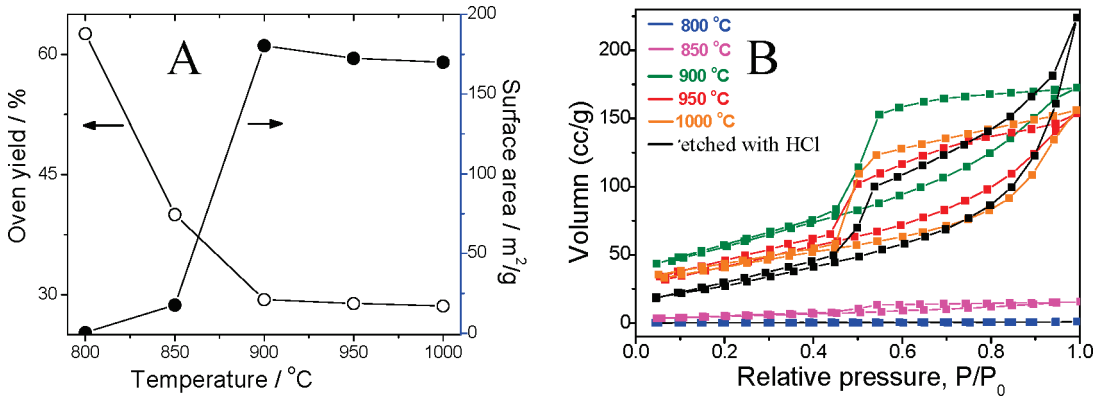

Figure 4. (A) Plots of the oven yield and surface area vs temperature and (B) nitrogen sorption isotherms of carbon products prepared at different temperatures in the presence of $FeCl_2 \cdot 4H_2O$. The black curve in part B is the carbon product (obtained at 1000 °C) after removal of iron species via HCl treatment.

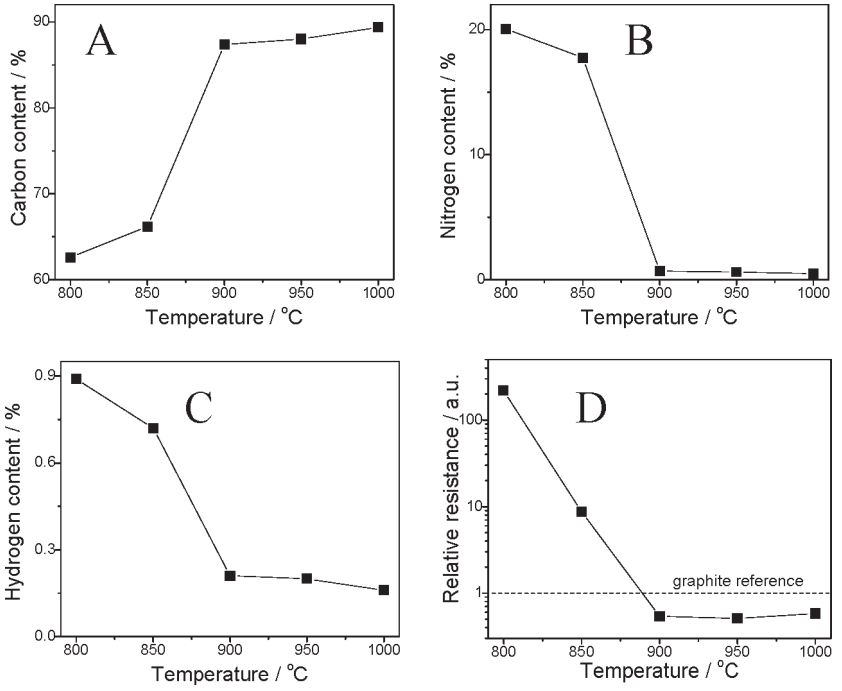

Figure 5. (A−C) Elemental (carbon, nitrogen, and hydrogen) analysis and (D) relative resistance of the products by pyrolyzing IL-b with 12 wt % $FeCl_2 \cdot 4H_2O$ at different temperatures from 800 to 1000 °C.

In Figure 4A, the oven yield and surface area of carbon products are plotted against temperature.

It is clearly seen that both curves behave in a nonlinear fashion, indicating the onset of a cooperative (simultaneous and relevant) process. The oven yield falls dramatically from 800 to 900 °C. One-third of the overall weight of the reaction mixture is lost in this narrow range, while elemental analysis indicates that, at this temperature, nearly all nitrogen is kicked out of the solid state structure. Above 900 °C, however, it stays almost constant. Parallel to the change of the oven yields, the BET surface areas underwent a similar change. At 800 °C, the surface area is close to 0. At 850 °C, a small surface area of 17.7 m^2/g is determined. It increases sharply up to 190.3 m^2/g at 900 °C, a level which is in fact kept at even higher temperatures.

The corresponding nitrogen sorption isotherms are displayed in Figure 4B. Below 900 °C, pore structures are apparently not developed. At 900, 950, and 1000 °C, the analysis of the isotherms indicates that the porosity of these materials spontaneously develops and is essentially made up of mesopores, with a negligible tiny fraction of macropores, only. It is to be pointed out that ordinary activated carbons are commonly microporous, while the present mesoporosity is favorable for a whole range of applications. The pore characteristics are independent of the temperature employed in the carbonization step, which means that they are rather stable, as expected for such graphitic nanostacks. The nitrogen sorption isotherms exhibit a type-H2 hysteresis loop with a pronounced desorption step. This is indicative of delayed capillary evaporation and the presence of constrictions in the mesopore structure (cagelike or bottle-like pores). In addition, all samples show a broad pore size distribution. All characteristics go well with a card-house structure of

graphitic nanostacks, as depicted within the TEM experiments.

The temperature dependent TEM images of the carbonized products with iron species from 800 to 950 °C are shown in Figure s2 in the Supporting Information. Once the carbonization temperature reaches 900 °C, the first metallic Fe-particles show up, and the curved, wrapped, and entangled graphitic stacks appear in the products. All these experiments clearly illustrate that carbon is crystallized at this distinct temperature

It was already stated that a deeper insight into the weight loss in the temperature range 800−1000 °C can be obtained from the elemental analysis of the carbon products. Figure 5A−C shows the curves of carbon, nitrogen, and hydrogen content vs temperature. Obviously, the carbon content increases in a phase-transition-like fashion with temperature from around 900 °C, while, complementarily, nitrogen and hydrogen decrease significantly at the same temperature step. This is followed by the relative resistance of the carbonized products. It drops by a factor of 25 times from 800 to 850 °C and another factor of 16 times from 850 to 900 °C. Above 900 °C, the relative resistance is lower than that of the graphite reference and remains constant.

It is clear that ordinary carbon does not crystallize that abruptly from more disordered and nitrogen containing precursors, and the presence of the Fe-catalyst must play a structure-decisive role. The very special role of iron and appropriate iron species is revealed by powder X-ray diffraction (XRD) on the diverse products obtained at different temperatures. First, it is clear that $FeCl_2 \cdot 4H_2O$ in IL-b will lose its hydration water while heating and will join the homogeneous weakly ordered glass or solid solution dominating the species up to 800 °C. From composition analysis, it is to be assumed also that the chlorine counterions have left the reaction mixture as HCl at those temperatures, making N^--species the effective counterions in the system.

As shown in Figure 6, at 800 and 850 °C, two reflection bands at 26° and 44° were observed in the XRD pattern. These two bands are rather broad, indicating rather disordered but mainly sp^2-hybridized carbon. No other reflections due to iron species were detected, supporting our view of the presence of a rather homogeneous solid solution. Once the temperature reached 900 °C, the broad peak at 26° becomes much sharper, indicating a rapid graphitization process starts at this temperature. Interestingly, there are additional reflections found which can be assigned to α-iron and iron carbide (Fe_3C) components in the product. It is well-known and a part of our engineering history that iron salts can be reduced to iron and then to iron carbide in the presence of carbon at elevated temperature, which is the so-called carbothermal reduction.[54] It is however obvious that, in the present case, the formation of iron and iron carbide nanoparticles and the graphitization are cooperative processes; that is, once the iron nanoparticles have been formed by reduction with the disordered carbon, they act vice versa as a catalyst for the formation of graphitic structures at

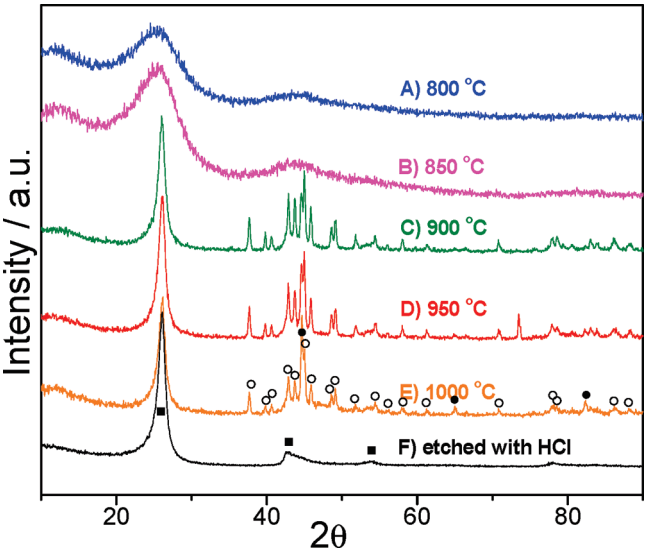

Figure 6. Powder X-ray diffraction patterns of carbon products from IL-b with $FeCl_2 \cdot 4H_2O$ at different temperatures: (A) 800; (B) 850; (C) 900; (D) 950; (E) 1000 °C. (F) Sample E after HCl treatment to remove iron and iron carbide: (graphitic phase, ■; iron, ●; and iron carbide, ○).

temperatures far below the standard graphitization temperatures (above 2000 °C) otherwise required in the absence of any catalyst. The formation of graphitic carbons from such nanoparticles usually takes place through a dissolution−precipitation mechanism that involves the dissolution of amorphous carbon into iron particles followed by the precipitation of graphitic carbon.[54,57] This is well-known from the formation of carbon nanotubes from the gas phase onto similar metal nanoparticles. In the present case of a solid state reaction, the graphitization reaction at 900 °C is so thoroughly and precisely conducted that a further increase in temperature to 950 and 1000 °C only results in slight changes of the product. In fact, it is this dissolution/reprecipitation process which also liberates the product from the larger amounts of nitrogen present in the primary product to be recrystallized, and it can be speculated that the perfection of the carbon structures formed is tightly coupled to the large extent of chemical leaving groups and the thereby promoted possibility of bond rearrangements. Comparable solid state reactions of nitrogen-poor precursors in the presence of iron salts result, in our experience,[58] only in less ordered carbon structures.

The iron and iron carbide nanoparticles within the mesoporous graphitic carbon products are accessible by external reactants. We proved that by an acid etching process of the sample pyrolyzed at 1000 °C. The etched sample, after washing and drying, was subjected to various characterizations. As shown in Figure 6F, the characteristic peaks of the graphitic phase remain after the etching process, while neither iron nor iron carbide were left.

(57) Huo, J.; Song, H.; Chen, X.; Zhao, S.; Xu, C. *Mater. Chem. Phys.* **2007**, *101*(1), 221–227.
(58) Adelhelm, P.; Hu, Y.-S.; Antonietti, M.; Maier, J.; Smarsly, B. M. *J. Mater. Chem.* **2009**, *19*(11), 1616–1620.

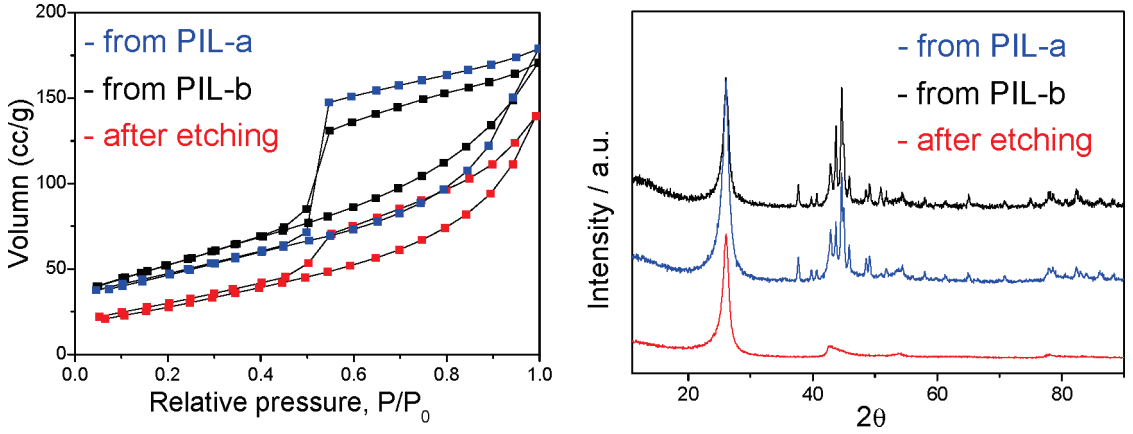

Figure 7. Nitrogen sorption isotherms (A) and XRD patterns (B) of carbon product from PIL-a (blue line) and PIL-b (black line) carbonized at 1000 °C with $FeCl_2 \cdot 4H_2O$. The black line represents the carbon product (PIL-b) after HCl etching.

We performed the TEM measurement on the etched samples and found only negligible trace of iron or iron carbide nanoparticles. HRTEM characterization (Figure 3B) confirms that the stacked graphene sheets in the lamellar-like graphitic nanostructures survive in the HCl etching process. Raman measurements of carbon samples before and after the acid etching were performed as well. The weak bands in the range 200−600 cm^{-1}, which are attributed to iron and iron carbide components,[59−61] vanish after the etching process, as expected. In addition, two strong bands were observed at 1346 and 1575 cm^{-1}, which are characteristic of a symmetry breakdown at the edge of graphene sheets (D band) and the E_{2g} vibrational mode of graphite layers (G band).[53] Two overtones and one combination of D and G bands were found at 2685, 3200, and 2925 cm^{-1}. The proportions of carbon in the graphitic and disordered forms, estimated from the integrated intensity ratio of G to D bands, are 52/48 and 58/42 before and after the etching process, respectively. The in-plane graphitic crystallite size (L_a) is calculated from these two ratios to be 4.8 and 6.1 nm ($L_a = 4.4(I_D/I_G)$).[62] The observation of a noticeable amount of disordered carbons or defects is related to the intrinsic graphitic nanostructures in our system: (1) the nanoscale thickness of the graphitic sheets makes the surface/volume ratio increase remarkably; (2) highly curved sheets introduce a large amount of grain boundaries. Due to the loss of iron and iron carbide nanoparticles during the etching process, the conductivity of the graphitic carbon decreases to a level which is slightly below that of dense commercial graphite powder; but the mesoporous nature is kept as a merit of our process. The BET surface area (Figure 4B black line) drops from 170 m^2/g (before etching) to 133 m^2/g afterward. The loss in surface area is believed to be due to the vanishing of iron and iron carbide nanoparticles, which contribute to the specific surface area. It should be kept in mind that both iron and iron carbide are important catalysts for many reactions, for example, the splitting of aqueous H_2O_2 to evolve oxygen.[46] In the present system, these nanoparticles are accessible and well-distributed in the mesoporous graphitic matrix. This makes the overall system a candidate for heterogeneous catalysis.

The influence of the amount of added $FeCl_2 \cdot 4H_2O$ on the carbon products (from IL-b) has been studied as well. For added weight fractions of 4% and 25% instead of 12%, a decrease of the BET surface area to 35 m^2/g and 100 m^2/g, respectively, was observed. Beside $FeCl_2 \cdot 4H_2O$, $CrCl_3 \cdot 6H_2O$ has also been tested in the carbonization process. It is found that, in the presence of 12 wt % of $CrCl_3 \cdot 6H_2O$, the carbon product shows a BET surface area of 145 m^2/g (nitrogen sorption isotherm in Figure s4 in the Supporting Information). It has been reported that both chromium and iron showed a higher catalytic activity than Ni and Co in the graphitization process.[52] Unfortunately, the chromium in the final carbon product occurs as a mixture of chromium carbide and chromium nitride, as determined from its XRD pattern (Figure s4 in the Supporting Information). The HCl etching procedure failed to remove it from the formed graphitic nanocomposite. In addition, because of its template-free character and easy implementation, the large-scale synthesis was tested as well. When the carbonization of IL-b in the presence of $FeCl_2 \cdot 4H_2O$ was scaled up by 25 times, we were able to synthesize as much as 2.75 g of carbon products (Figure s5 in the Supporting Information).

A key issue and experimental handle in the present approach is the ability to move from IL monomers to PIL polymers. We actually expect that the carbonization takes place in an unaltered fashion, as the IL monomers, prior to the pyrolysis, will thermally polymerize into polymers in early stages of the reaction. Nevertheless, starting from an already prepolymerized monomer allows typical polymer operations, such as molding, extrusion, coating, or casting under preservation of a given shape (contrary to low molecular weight liquids). Such a structured polymer film could then be transferred in a ceramic-like processing step into the final carbon structure.

(59) Stanghellini, P. L.; Sailor, M. J.; Kuznesof, P.; Whitmire, K. H.; Hriljac, J. A.; Kolis, J. W.; Zheng, Y.; Shriver, D. F. *Inorg. Chem.* **1987**, *26*(18), 2950–4.
(60) Park, E.; Zhang, J.; Thomson, S.; Ostrovski, O.; Howe, R. *Metall. Mater. Trans. B* **2001**, *32B*(5), 839–845.
(61) Yastrebov, S. G.; Ivanov-Omskii, V. I.; Kosobukin, V. A.; Dumitrache, F.; Morosanu, C. *Tech. Phys. Lett.* **2004**, *30*(12), 995–997.
(62) Tuinstra, F.; Koenig, J. L. *J. Chem. Phys.* **1970**, *53*(3), 1126–30.

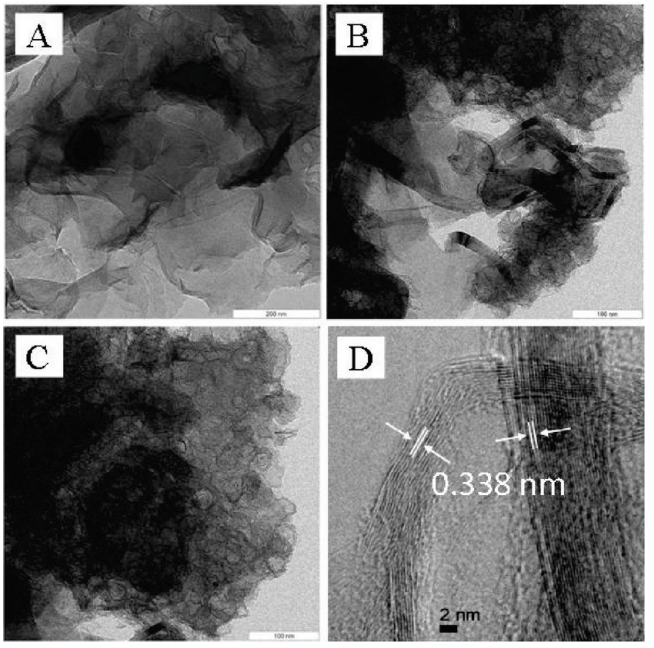

Figure 8. TEM images of carbon products from PIL-a (A) and PIL-b (B and C). D is a HRTEM image of a carbon product from PIL-b. The scale bars are 200, 100, 100, and 2 nm, respectively.

To verify this assumption, two homopolymers of poly(IL-a) (PIL-a) and poly(IL-b) (PIL-b) were prepared by conventional free radical polymerization of IL-a and IL-b, respectively. The carbonization is conducted in the same way as that of the monomers. Indeed, the yields, physical properties, and chemical composition of the carbon products derived from PIL homopolymers are very close to those of the corresponding IL monomers. They are nonporous ($S_{BET} < 10\ m^2/g$) when carbonized in the temperature range from 800 to 1000 °C without $FeCl_2 \cdot 4H_2O$, and turned mesoporous in the presence of $FeCl_2 \cdot 4H_2O$ (12 wt %). Figure 7A shows their nitrogen sorption isotherms of the carbon products obtained at 1000 °C with $FeCl_2 \cdot 4H_2O$. As determined, the carbon products from PIL-a and PIL-b exhibit a surface area of 164 and 188 m^2/g, respectively, close to that of their corresponding monomers (220 and 170 m^2/g). Their XRD patterns display the reflection peaks of the graphitic phase, iron and iron carbide, as we expected. The carbon products show a relative resistance of 0.55 and 0.69, respectively. The acid etching process was performed on the carbon product prepared from PIL-b. The etched product is practically purely in the graphitic phase, as confirmed by the XRD pattern in Figure 7. This indicates that the iron and iron carbide nanoparticles in the carbon product obtained from PIL polymers were accessible as well. The nitrogen sorption isotherm of the HCl-etched product is shown in Figure 7A. A surface area of 106 m^2/g is determined.

The TEM characterization of the two carbon products was conducted to check the state of development of the graphitic structures. Figure 8A shows a representative TEM image of the carbon product from PIL-a. It exhibits also flat but folded graphitic nanostack structures, close to that of monomer IL-a. Interestingly, the carbon product from PIL-b (Figure 8B) shows two coexisting but related carbon textures, i.e. highly wrapped layer stacks and bubble-like vesicles, which were not found for the monomer IL-b. The thickness of the wrapped stacks is 5−20 nm, and that of the bubble wall is 5−10 nm. Some fully developed bubble morphologies can also be observed, as shown in Figure 8C. HRTEM characterization (Figure 8D) reveals that all these textures are made up of stacked graphene sheets with a spacing of 0.338 ± 0.002 nm. In spite of these large and expected similarities between using IL monomer and polymer as precursors for the pyrolytic formation of mesoporous graphitic carbons, we can take the concept of PIL polymers to be proven.

4. Conclusions

We demonstrated a template-free procedure to prepare highly conductive mesoporous graphitic carbon nanostructures by using ionic liquid monomers or poly(ionic liquid) polymers as carbon precursors in the presence of $FeCl_2 \cdot 4H_2O$. IL and PIL play the role of a convenient carbon precursor with minimal vapor pressure until the onset of decomposition, and appropriate choice of both monomer and counterion allows for optimization of the carbon yield. In the following graphitization process, $FeCl_2$ as metal salt source plays a key role in conducting the crystallization toward graphitic structures at moderate temperatures (900−1000 °C). A detailed investigation on the carbonization process demonstrated that 900 °C is the threshold at which the graphitization process took place in a stepwise fashion and the superior physical properties developed, such as high surface area and low electric resistance. It was proven that this is due to the onset of carbothermal reduction of Fe^{2+} toward iron and iron carbide nanoparticles, which act via a dissolution/reprecipitation process as the active recrystallization medium. Via acid etching, iron and iron carbide nanoparticles could be removed, leaving pure mesoporous graphitic nanomaterials with rather well developed graphitic stacks of 5−20 nm thickness. As a consequence of the template-free character of the process, it is easy to implement and scale up.

Ongoing work is related to raise added benefits of the polymer by coupling polymer micro- and nanoprocessing with this cooperative bottom up structure formation. In addition, we will analyze the potential of the as-synthesized carbon products, such as for use in catalysis, as anode material for fuel cells, or as supercapacitors.

Acknowledgment. J.Y. would like to thank the Max Planck Society for financial support, Dr. A. Garcia Marquez and A. Kraupner for the XRD measurements and the HCl etching process, J. Weber and R. Regina for helpful discussions about the nitrogen sorption measurement, and the Fritz Haber Institute of the Max Planck Society/Berlin for HR-TEM measurements.

Supporting Information Available: Additional figures showing the following: (1) representative TEM images of iron and iron

carbide nanoparticles in the graphitic matrix; (2) TEM images of the carbon products prepared from IL-b with $FeCl_2 \cdot 4H_2O$ at temperatures from 800 to 950 °C, and the carbon products (pyrolyzed at 1000 °C with $FeCl_2 \cdot 4H_2O$) after removal of iron species; (3) Raman spectra of the carbon products (pyrolyzed at 1000 °C with $FeCl_2 \cdot 4H_2O$) before and after removal of iron species; (4) XRD pattern and nitrogen sorption isotherm of the carbon product obtained from the carbonization of IL-b in the presence of $CrCl_3 \cdot 6H_2O$ (12 wt %) at 1000 °C; (5) photograph and TEM image of the carbon products synthesized in large scale (PDF). This material is available free of charge via the Internet at http://pubs.acs.org.